IEEE Open Journal of Nanotechnology

Received 2 September 2022; revised 18 September 2022; accepted 21 September 2022. Date of publication 28 September 2022; date of current version 17 October 2022. The review of this article was arranged by Associate Editor Masaharu Shiratani.

Digital Object Identifier 10.1109/OJNANO.2022.3209995

Plasma Synthesis of Silicon Nanoparticles: From Molecules to Clusters and Nanoparticle Growth

SHOTA NUNOMURA [1], KUNIHIRO KAMATAKI [2], TAKEHIKO NAGAI [3], TATSUYA MISAWA [4], SHINJI KAWAI [5], KOSUKE TAKENAKA [6], GIICHIRO UCHIDA [7], AND KAZUNORI KOGA [2]

[1]Research Institute for Advanced Electronics and Photonics, National Institute of Advanced Industrial Science and Technology, Tsukuba, Ibaraki 305-8568, Japan
[2]Graduate School of Information Science and Electrical Engineering, Kyushu University, Nishi-ku, Fukuoka 819-0395, Japan
[3]Research Institute for Energy Conservation, National Institute of Advanced Industrial Science and Technology, Tsukuba, Ibaraki 305-8568, Japan
[4]Faculty of Science and Engineering, Saga University, Saga 840-8502, Japan
[5]Industrial Technology Center of Saga, Saga 840-0932, Japan
[6]Joining and Welding Research Institute, Osaka University, Ibaraki, Osaka 567-0047, Japan
[7]Faculty of Science and Technology, Meijo University, Tempakuku, Nagoya 468-8502, Japan

CORRESPONDING AUTHOR: SHOTA NUNOMURA (e-mail: s.nunomura@aist.go.jp)

This work was supported by JSPS KAKENHI under Grant 18K03603.

ABSTRACT Plasma nanotechnology is widely used for nanoscale etching, dopant implantation and thin-film deposition for state-of-the-art semiconductor devices. Such a plasma nanotechnology has another interesting aspect of synthesizing nanoparticles, in a controlled manner of atomic composition, structure and those size. Here, we present the polymerization and growth of silicon nanoparticles from a molecular level to 10 nm-particles in hydrogen diluted silane plasmas. The polymerization and growth are experimentally studied using various plasma diagnostic tools. The results indicate that nanoparticles are rapidly formed via gas-phase reactions in a low-density plasma comprising high-energy electrons. The growth kinetics and the modification of plasma properties are discussed in terms of gas-phase reactions, charging and coagulation of nanoparticles.

INDEX TERMS Silicon nanoparticles, silane plasmas, quantum dots, solar cells, lithium ion battery.

I. INTRODUCTION

In recent years, silicon (Si) nanoparticles [1], [2], [3], [4], [5] have been of great importance on quantum computing, third-generation solar cells, and high-performance lithium ion batteries (LIBs). For example, in quantum computing devices [6], [7], [8], Si nanoparticles can be used as quantum dots (QDs), where electrons are confined and spins are controlled for computing. For solar cells [9], [10], [11], Si nanoparticles of QDs are expected to yield the multiple exciton generation (MEG) for boosting the efficiency beyond the Shockley-Queisser limit. In LIBs [12], [13], [14], [15], the Si nanocomposite anode is demonstrated to increase the specific capacity and cyclic performance, by replacing the current anode of graphite. The Si nanoparticles are also employed for luminescence, where the bandgap engineering is performed to obtain the blue luminescence [16], [17]. For these devices, the size of Si nanoparticles is crucial, which frequently governs the device performances.

Si nanoparticles can be synthesized by several methods: evaporation [18], laser ablation [19], [20], electrochemical etching [21], and plasma nanotechnology [22], [23], [24]. Among them, the plasma nanotechnology has an advantage for precisely controlling the atomic composition, structure and size of nanoparticles. So far, the structure-controlled Si nanoparticles such as amorphous or crystallined have been successfully synthesized in a wide range of sub-nanometers to hundreds of nanometers, by three orders of magnitude, by simply changing the period of synthesis from milliseconds to hundreds of seconds [22], [23], [24]. Two examples for those Si nanoparticles are shown in Fig. 1, where ≈20 nm-amorphous or ≈2 nm-crystallined particles are nicely formed. Nevertheless, the details of the formation mechanism

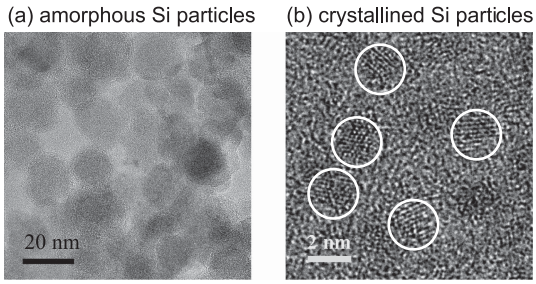

FIGURE 1. Transmission electron microscope (TEM) images of (a) amorphous silicon (Si) nanoparticles and (b) crystallined Si nanoparticles, synthesized in silane plasmas [22], [23], [24].

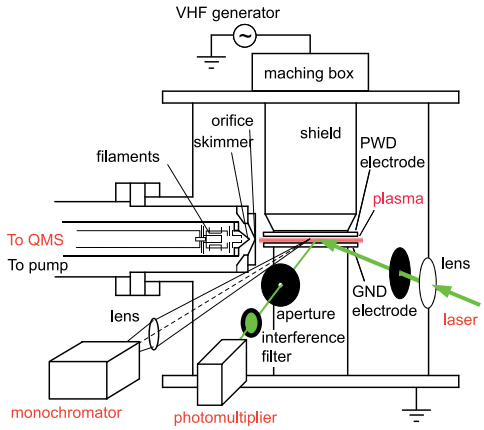

FIGURE 2. Experimental setup. Si nanoparticles are synthesized from a source gas of silane (SiH_4) diluted with hydrogen (H_2) in capacitively-coupled discharge plasma. The plasma is diagnosed by quadruple mass spectrometry (QMS), optical emission spectroscopy (OES) and laser light scattering (LLS) for nanoparticle detection.

of nanoparticles, i.e., the polymerization and growth kinetics, are not fully understood. This is because the gas-phase reactions in those plasmas are highly complicated, and a variety of radicals, polymerized species of ions and neutrals as well as clusters are coexisted, interacting one to another [25], [26].

In this paper, we present the polymerization and nanoparticle growth in hydrogen-diluted silane plasmas, generated by very-high-frequency (VHF) discharge. The plasmas are diagnosed by the conventional methods of quadruple mass spectrometry, optical emission spectroscopy and laser light scattering for nanoparticle detection. The time evolutions of the gas-phase composition including polysilane molecules and nanoparticles are measured. Based on the measurements, the polymerization and nanoparticle growth are discussed via examining the densities of various gas-phase species and the reaction rates of those species in plasmas.

II. EXPERIMENTAL

A. DISCHARGE AND PLASMA PARAMETERS

The experiments of nanoparticle growth are performed in capacitively-coupled 60-MHz-VHF discharge in a parallel-plate configuration [27], [28], as shown in Fig. 2. Two electrodes of powered (PWD) and electrically grounded (GND) are placed at the center of a vacuum chamber, and separated at a distance of 6 mm for discharge. The discharge gas, i.e., a source gas of nanoparticles, is silane (SiH_4) diluted with hydrogen (H_2). The source gas is introduced from the PWD electrode shower head, and pumped out through a side port. The SiH_4 and H_2 gas flows are 2 sccm and 98 sccm, respectively; the H_2 dilution is 50. The gas pressure is controlled at 5.0 Torr. A SiH_4/H_2 discharge plasma is generated by applying a peak-to-peak voltage of $V_{pp} = 260$ V to the PWD electrode. The discharge power is 100 W (0.78 W/cm^2) for this V_{pp}. The discharge period is set at 2.0 s. The electrode and chamber wall are not heated; those are kept at room temperature.

For the present configuration of discharge, the discharge is symmetric [29]. The self-bias is nearly zero on the PWD electrode. The time-averaged plasma potential is thus given by one forth of V_{pp}, i.e., $\approx$65 V. The plasma density is obtained to be $\approx 10^{10}$cm^{-3} from the ion saturation current for H_2 discharge [27]. The electron temperature is estimated to be roughly 0.8 eV for H_2 discharge [27].

B. PLASMA DIAGNOSTICS

The SiH_4/H_2 discharge plasma is diagnosed with conventional methods: quadruple mass spectrometry (QMS), optical emission spectroscopy (OES) and laser light scattering (LLS) for nanoparticle detection. The QMS is used for measuring the gas composition and ion species [30], [31]. The QMS tube is differentially pumped, down to $\lessapprox 10^{-6}$ Torr for operation (see Fig. 2 on the left-hand side). The orifice and skimmer are mounted on the tube head. The orifice and skimmer hole diameters are 300 μm and 200 μm, respectively. The QMS signals are detected for silane, di-silane (Si_2H_6) and tri-silane (Si_3H_8) molecules at mass numbers of 30, 60 and 90, respectively. To obtain the time evolutions of these species, the signals are recorded at an acquisition rate of 43 ms.

From OES, the radical generation is monitored throughout discharge. The hydrogen Balmer series [32], H_α at 656.3 nm and H_β at 486.1 nm, are measured to confirm the existence of H radicals. The intensity ratio of H_β to H_α, $I_{H\beta}/I_{H\alpha}$, is calculated for monitoring the high-energy tail of the electron energy distribution function (EEDF), which is related to the dissociation and ionization of molecules. The optical emission at 414 nm [33], I_{SiH}, is measured for the detection of SiH radicals, which are one of the dissociation fragments of SiH_4.

C. NANOPARTICLE DETECTION

The LLS is performed to detect nanoparticles growing in the plasma [34], [35]. The laser light operated at 532 nm and 1.0 W is injected near the plasma sheath edge of the PWD electrode through an aperture with a focus lens. The light scattered from nanoparticles is detected with a photomultiplier at the angle of 90° from the incident light, through another aperture and interference filter. The LLS intensity, I_{LLS}, reflects the amount of nanoparticles, which is proportional to the nanoparticle density, n_p, and the sixth power of the nanoparticle diameter, d_p, i.e., $I_{LLS} \propto n_p d_p^6$, for Rayleigh scattering.

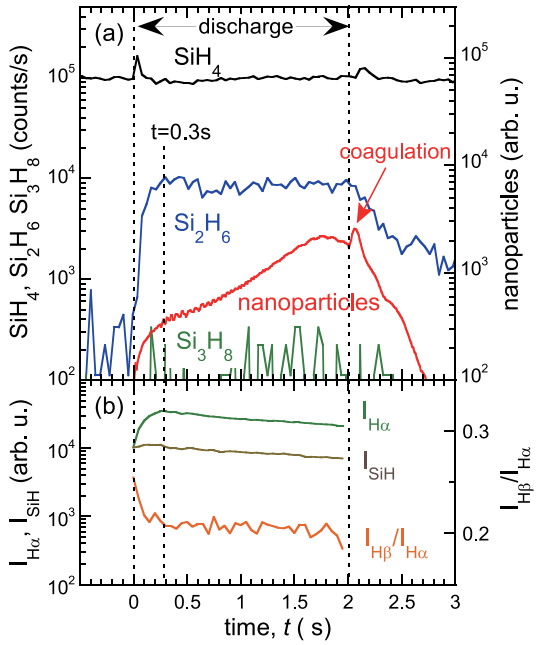

FIGURE 3. **Time evolutions of (a) gas-phase species and (b) optical emission. Polysilane molecules of disilane (Si_2H_6) and trisilane (Si_3H_8) are rapidly generated at the beginning of discharge. Nanoparticle amount is increased with the discharge time, *t*.**

In this study, both d_p and n_p are consistently determined from the coagulation dynamics of nanoparticles. Such coagulation is triggered by the termination of discharge. The coagulation results in an increase of the LLS intensity, from which both d_p and n_p are computed, using a formula of Rayleigh scattering and mass conservation equation. The details for the determination of d_p and n_p are described in a reference [34].

III. RESULTS

A. TIME EVOLUTIONS OF GAS-PHASE SPECIES AND OPTICAL EMISSION

The time evolutions of the gas composition and nanoparticle amount are shown in Fig. 3(a). The discharge is initiated at $t = 0.0$ s and terminated at $t = 2.0$ s. As shown, the density of SiH $_4$ is confirmed to be constant during the discharge; the depletion of SiH_4 is not observed. For Si_2H_6 molecules, they are efficiently generated at the early period of discharge ($t \lessapprox 0.3$ s, denoted by a dashed line). The density of Si_2H_6 reaches to one tenth of that of SiH_4 in the later period of discharge ($t \gtrapprox 0.3$ s). The generation of Si_3H_8 is also observed, however the density is low; it is roughly two order of magnitude smaller than that of SiH_4. As for nanoparticles, the LLS intensity is rapidly increased with the discharge time, t, for $t \lessapprox 0.3$ s, which reflects an increase in the nanoparticle diameter. Later, the LLS intensity is gradually increased, and a small oscillation is observed, indicating the excitation of so-called dust acoustic waves [40], [41]. After the termination of discharge, the LLS intensity is slightly increased in a short period of 0.1 s (denoted by arrow), which implies the coagulation of nanoparticles. This coagulation is induced by the thermal motion of nanoparticles, which is suppressed by repulsive Coulomb interaction among charged nanoparticles during discharge. The details of charging and coagulation are discussed in Section IV. The LLS intensity is finally monotonically decreased, indicating the diffusion of nanoparticles and the removal from the discharge gap [42].

Figure 3(b) shows the time evolutions of OES signals. Carefully looking at the data, the following interesting feature is recognized. At the early period of discharge ($t \lessapprox 0.3$ s), $I_{H\alpha}$ is low and $I_{H\beta}/I_{H\alpha}$ is high, comparing to those in the later period ($t \gtrapprox 0.3$ s). This low $I_{H\alpha}$ suggests a low-density plasma, since $I_{H\alpha}$ is primarily proportional to the electron density [36]. A high number of $I_{H\beta}/I_{H\alpha}$ reflects the presence of high-energy electrons, because higher excited states of H are generated more by high-energy electrons via the electron impact dissociation of H_2 [37]. So, the observed low $I_{H\alpha}$ and high $I_{H\beta}/I_{H\alpha}$ indicate a low-density plasma comprising high-energy electrons. Such a plasma is considered to be formed by containing a large amount of nanoparticles. When a large amount of nanoparticles are formed in a plasma, a fraction of nanoparticles are negatively charged [38], via the electron attachment on the particle surface. This electron attachment is enhanced for low-energy electrons because of the polarization effect of nanoparticles, similar to the formation process of negative ions [39]. The charging of nanoparticles induces the collection of positive ions, causing the recombination between electrons and positive ions on the nanoparticle surface. As a result, the electron density is simply lowered and the high-energy electrons remain to sustain the discharge. This point is discussed more in Section IV. For I_{SiH}, it shows a slightly decreasing tendency during the discharge, which implies the generation rate of SiH_m radicals via the electron impact dissociation of SiH_4 is slightly reduced.

B. NANOPARTICLE DIAMETER AND DENSITY

For the nanoparticles, both d_p and n_p are determined from the LLS intensity. The results are shown in Fig. 4(a). As shown, d_p is increased with t, while n_p is decreased. Specifically, d_p is increased from $\approx$2.0 nm at $t = 15$ ms to $\approx$10 nm at $t = 0.3$ s, and n_p is decreased from $\approx 10^{12}$ cm^{-3} at $t = 15$ ms to $\approx 3 \times 10^{10}$ cm^{-3} at $t = 0.3$ s. From this data, the growth rate of nanoparticles is calculated by a linear fit (indicated by a dashed line), and it gives 34.8 nm/s. Interestingly, a linear fit gives a constant value of $\approx$ 1.9 nm, which implies the existence of nuclei of nanoparticles, often called clusters [24]. The d_p and n_p data imply that those clusters are fairly rapidly formed ($\lessapprox$15 ms) at a high density of $\approx 10^{12}$ cm^{-3}. The details of the formation of clusters and nanoparticle growth are discussed later in Section IV. The volume fraction of nanoparticles is calculated by $4\pi/3(d_p/2)^3 n_p$, which is plotted in Fig. 4(b). The volume fraction is increased with t and saturated for the later period. It varies in a range of 10^{-9} to 10^{-8}.

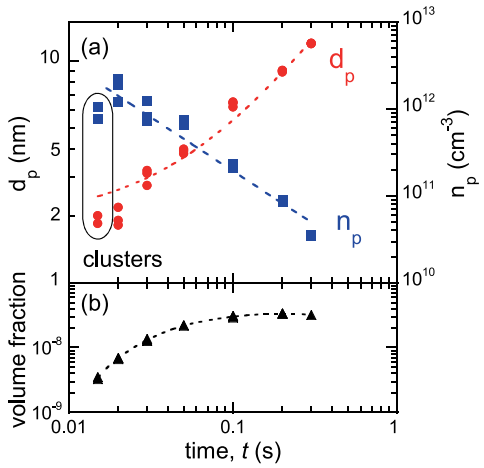

FIGURE 4. (a) Time evolutions of nanoparticle diameter, d_p, and density, n_p. With increasing t, d_p is increased and n_p is decreased. A liner fit of d_p, denoted by a dashed line, yields a constant value of 1.9 nm, which implies the existence of clusters at the beginning of discharge. (b) Nanoparticle volume fraction.

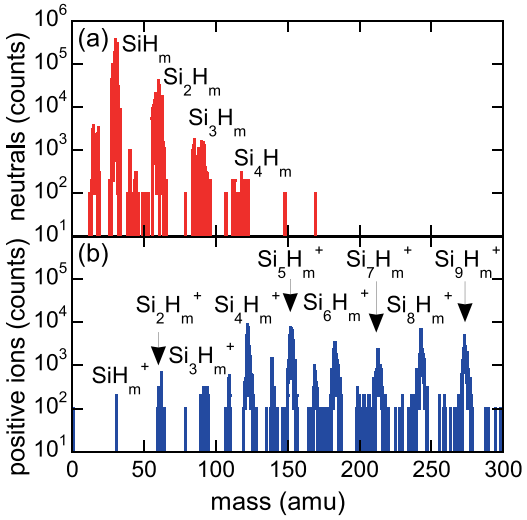

FIGURE 5. Mass spectra of (a) neutrals and (b) ions. The spectra are different between them, indicating a different channel of polymerization for neutrals and ions.

C. MASS SPECTRA OF NEUTRALS AND IONS

The mass spectra of natural and ion species are measured for a long period of discharge (10 min). These are shown in Fig. 5. For the naturals (Fig. 5(a)), polysilane molecules of Si_2H_6, Si_3H_8 and Si_4H_{10} are detected. The densities of these molecules are estimated from the spectrum intensity, by comparing to the intensity of SiH_4. The density of SiH_4 is known from the gas pressure, and it is $\approx 3.22 \times 10^{15}$ cm^{-3} for the present condition of 5.0 Torr and a H_2-dilution ratio of 50. So, the densities of polysilane molecules are deduced to be $\approx 10^{14}$ cm^{-3} for Si_2H_6, $\approx 10^{13}$ cm^{-3} for Si_3H_8 and $\approx 10^{12}$ cm^{-3} for Si_4H_{10}, respectively. These numbers are listed in Table 1.

TABLE 1. Densities of Gas-Phase Species in SiH_4/H_2 Plasmas

species	density (cm^{-3})	comments
electrons	$\approx 10^{10}$	for H_2 plasma
positive ions ($Si_nH_m^+$)	$\lessapprox 10^{10}$	
negative ions ($Si_nH_m^-$)	$\lessapprox 10^{10}$	by QMS [39]
radicals (SiH_3)	$\approx 10^{12-13}$	cavity ring-down [52]
radicals (SiH_2)	$\approx 10^{9}$	interacavity laser absorption [53]
radicals (SiH & Si)	$\approx 10^{8-9}$	laser-induced fluorescence [51]
H	$\approx 10^{12}$	for H_2 plasma [47]
H_2	1.57×10^{17}	from pressure
SiH_4	3.22×10^{15}	from pressure
Si_2H_6	$\approx 10^{14}$	from QMS
Si_3H_8	$\approx 10^{13}$	from QMS
Si_4H_{10}	$\approx 10^{12}$	from QMS
clusters	$\approx 10^{12}$	from LLS
nanoparticles	$\approx 10^{10-12}$	from LLS

The mass spectrum of ion species is shown in Fig. 5(b), which is fairly different from that of neutrals, described above. The polysilane ions up to $Si_9H_m^+$ are clearly observed. The monosilane ions (SiH_m^+) are detected, however the density is low, although SiH_m^+ are initially generated by electron impact ionization of SiH_4 [43] and/or the reactions between hydrogen ions of H_3^+ and SiH_4, i.e., $H_3^+ + SiH_4 \rightarrow SiH_3^+ + 2H_2$ [44]. These observations indicate that the polysilane ions are not generated via the electron impact ionization of the polysilane molecules. Instead, the polysilane ions are generated via the ion-molecule reaction of $Si_nH_m^+ + SiH_4 \rightarrow Si_{n+1}H_l^+ + jH_2 + kH$, where $m + 4 = 2j + k + l$ [45], [46]. This SiH_4 addition reaction is known to have a high rate constant of $k \gtrsim 10^{-11}$ cm^3/s [25], [26]. For these positive ions, the density in total is expected to be of the order of $\lessapprox 10^{10}$ cm^{-3} from the simulation [47] and a measurement [27] for H_2 discharge, which is listed in Table 1. The density of positive ions is thus lower than those of polysilane molecules, clusters and nanoparticles, by two order of magnitude. So, the clusters and nanoparticles are mostly neutral; a fraction (a few-%) of those are charged.

IV. DISCUSSION

Here, we discuss the polymerization and nanoparticle growth observed in the present SiH_4/H_2 plasmas. To do that, we briefly describe the elementary processes in those plasmas and summarize the densities of various neutral and ion species (Table 1). Then, we examine the reaction rate constants of reactive species for polymerization and nanoparticle growth. The roles of hydrogen atom (H), charging, coagulation of nanoparticles and the property of a plasma containing nanoparticles are also discussed.

A. ELEMENTARY PROCESSES

In SiH_4/H_2 plasmas, the electron impact on SiH_4 [48], [49] or H_2 [50] results in either ionization, dissociation, electron attachment or excitation [51], as shown in Fig. 6 (the upper part). In general, these elementary processes are highly dependent on the incident energy of electrons. For low-energy

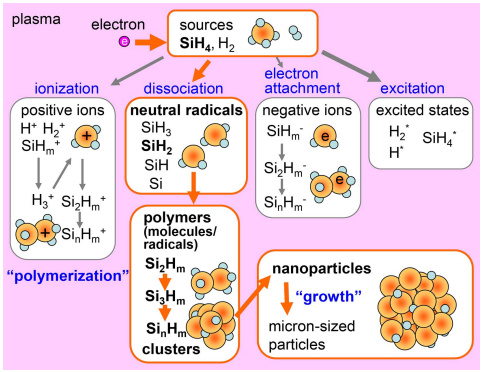

FIGURE 6. Model of polymerization and nanoparticle growth. The elementally processes in SiH_4/H_2 plasmas are shown in the upper part. The polymerization of neutrals is primarily owing to the SiH_2 insertion reaction, which brings the formation of clusters, i.e., the nuclei of nanoparticles (shown in lower-middle). The nanoparticles are grown by the deposition of SiH_3 precursors on their surface (shown in lower-right).

electrons ($\lessapprox$ a few eV), the molecular excitation is dominant. However, for the energy of ≈10 eV or higher, the dissociation becomes dominant over the other processes. The electrons with such energies are abundant in the present plasma, so that SiH_4 and H_2 are efficiently dissociated. The dissociation is confirmed by OES, shown in Fig. 3(b), where the existence of H and SiH radicals are recognized.

The electron-impact dissociation of SiH_4 generates SiH_m radicals: e + SiH_4 → SiH_m + jH_2 + kH + e, where $4 = m + 2j + k$. Among SiH_m radicals, SiH_2 and SiH_3 are preferentially generated (the blanching ratio is 43% for SiH_2, 36% for SiH_3, 12% for SiH and 9% for Si at 70 eV) [25], [43]. The SiH_2 radicals are highly reactive, and they are rapidly converted into Si_2H_6 via the insertion reaction with SiH_4: $SiH_2 + SiH_4 \rightarrow Si_2H_6$ [25], [26]. The rate constant for this reaction is 4.6×10^{-10} cm^3 s^{-1} at 500 K [25], [26], which is significantly high, compared with the other reactions of yielding Si_2H_6 such as $SiH_3 + SiH_3 \rightarrow Si_2H_6$ ($\approx 10^{-11}$ cm^3 s^{-1}) [26]. This SiH_2 insertion reaction can be confirmed by the time evolution of gas-phase species, shown in Fig. 3(a), where Si_2H_6 molecules are observed at the very beginning of discharge and those density is relatively high. Because of this insertion reaction, the density of SiH_2 is lowered, comparing to that of SiH_3 (as listed in Table 1), although the blanching ratio is similar, described above. The SiH_3 radicals may react with SiH_4 molecules, however the resultant are mainly SiH_3 radicals. So, the density of SiH_3 is not lowered by this SiH_3-SiH_4 reaction.

B. POLYMERIZATION

The SiH_2 radicals are also highly reactive with Si_2H_6, Si_3H_8, and other polysilane molecules of Si_nH_{2n+2}, observed in the mass spectrum (Fig. 5(a)). So, the SiH_2 insertion reaction induces the polymerization of these molecules: $SiH_2 + Si_nH_{2n+2} \rightarrow Si_{n+1}H_{2n+4}$. The polymerization based on this SiH_2 insertion reaction is considered to continue until the polysilane molecules become large enough, regarded as clusters, i.e. nuclei of nanoparticles [22], [23], [24]. The clusters are composed of several tens to hundreds of Si atoms, and the size of clusters may range from sub-nanometers to a few nanometers. In the experiment, the formation of clusters is implied from the time evolution of d_p in Fig. 4(a), where d_p remains a constant $t \lessapprox 15$ ms. From the data, the clusters of 1.9 nm in diameter are rapidly formed at a high density of $\approx 10^{12}$ cm^{-3}.

C. NANOPARTICLE GROWTH

Once the clusters are formed, the insertion reaction of SiH_2 becomes less dominant. Instead, the deposition of SiH_3 radicals on the surface of clusters becomes dominant [22], [23], [24]. The density of SiH_3 [52] is higher than that of SiH_2 [53] by three to four order of magnitude, thus the deposition precursors are regarded as SiH_3 radicals. The deposition rate, DR, can be estimated from the flux of SiH_3 radicals, and given by $DR = \gamma_s n_{SiH3} v_{th} \Delta V_{Si}$, where γ_s is the sticking probability, n_{SiH3} is the density of SiH_3, v_{th} is the thermal velocity, and ΔV_{Si} is the volume of a single Si atom occupying in diamond structure of lattice. With $\gamma_s = 0.09$ [54], [55], n_{SiH3} $\approx 10^{13}$ cm^{-3} [52], $v_{th} = 4.7\times10^4$ cm/s, and $\Delta V_{Si} = 2.0 \times 10^{-23}$ cm^3, the deposition rate is calculated to be $DR \approx$ 8.5 nm/s. The growth rate of nanoparticles is then given by multiplying a factor of 2 to DR, taking account of the front- and rear-side deposition of nanoparticles: $GR = 2 \times DR$. Under the present experimental condition, the growth rate is estimated to be $GR \approx 17.0$ nm/s, which roughly agrees with a measurement value of 34.8 nm/s, at least in terms of the order of magnitude. The difference in factor of two may come from the ambiguity of those values of γ_s on the nanoparticle surface and n_{SiH3} for the current high-H_2 dilution. This ambiguity is discussed in the next section.

D. ROLES OF HYDROGENS

The H atoms play important roles in the reaction kinetics in SiH_4/H_2 plasmas. They are generated mainly by the electron impact dissociation of H_2 for a high-H_2 dilution condition. The density of H is measured to be of the order of 10^{12} cm^{-3} for a H_2 plasma [47] (as listed in Table 1) under a condition similar to the present experiment. The generated H atoms react with SiH_4 molecules, yielding the SiH_3 radicals: $H + SiH_4 \rightarrow H_2 + SiH_3$, where the rate constant is 1.2×10^{-9} $cm^3 s^{-1}$ at 500 K [25], [26]. So, SiH_3 radicals are efficiently generated by this reaction, in addition to the election impact dissociation of SiH_4, described above. This additional generation of SiH_3 radicals contributes to the growth of nanoparticles, via the deposition on the nanoparticle surface.

The H atoms also impact on the growth rate of nanoparticles via the modification of γ_s. In the previous section, $\gamma_s = 0.09$ is used to examine GR, although it's value is obtained in SiH_4 plasmas for a low-H atom density. The H atoms are known to react with the surface Si-H bonds of nanoparticles, generating the Si dangling bonds on the surface, i.e., the reaction sites for SiH_3 radicals [25]. Because of that, γ_s of the nanoparticle surface is expected to be increased for SiH_4/H_2 plasmas under a high-H_2 dilution condition. This effect of increased γ_s may

explain the discrepancy of *GR* between the estimation and observation by a factor of two.

Besides, the H atoms have a strong impact on the structure of nanoparticles, i.e., amorphous or crystallined, as shown in Fig. 1. It is known that crystallined Si nanoparticles are formed under a very high-H_2 dilution of $\gtrapprox$100 [1]. The mechanism for the crystallization of Si nanoparticles is still not clear. Nevertheless, it can be closely related to the reorganization of bond configurations in amorphous network by H atoms. For the present experiment, amorphous nanoparticles are considered to be mainly formed.

E. CHARGING AND PROPERTY OF PLASMAS

The charging of nanoparticles strongly modifies the property of plasmas. As listed in Table 1, the density of nanoparticles is significantly higher than those of electrons and ions. So, a fraction of nanoparticles are charged. The charging of nanoparticles is primarily caused by either electron or ion attachment. Because of the difference of thermal velocities between them, nanoparticles are charged negatively via electron attachment. The electron attachment is considered to be highly dependent on the energy of electrons, similar to the negative ion formation [39], where the polarization plays an important role. The electron attachment can be enhanced for low-energy electrons because of the polarization effect of nanoparticles. Once nanoparticles are charged negatively, they efficiently collect positive ions via attractive Coulomb interaction, inducing the recombination of electrons and positive ions. This recombination causes a reduction in the plasma density, indicated by the observation of a low number of $I_{H\alpha}$ in the early period of discharge. The electron attachment is thus prominent for low-energy electrons, and therefore high-energy electrons remain in a low-density plasma to sustain the discharge, as indicated by a high number of $I_{H\beta}/I_{H\alpha}$ (see Fig. 3(b)).

F. COAGULATION OF NANOPARTICLES

The coagulation of nanoparticles is indicated by an increase in the LLS intensity after the termination of discharge (Fig. 3(a), denoted by arrow). This coagulation is induced by the thermal motion of nanoparticles. During discharge, the nanoparticles are charged negatively, as mentioned above, and thereby the coagulation is suppressed via the repulsive Coulomb interaction. The suppression of coagulation even works for nanoparticles, where a fraction of them are charged. This is because the charging of nanoparticles is faster than the collision among nanoparticles, as described in a reference [1], [38]. After the termination of discharge, the charged nanoparticles are neutralized, and then they begin to collide each other via their thermal motion, i.e., coagulation. The coagulated particles are observed by TEM under a similar condition, which is shown in Fig. 1(a).

V. CONCLUSION

The polymerization and nanoparticle growth are experimentally studied in a VHF discharge plasma of SiH_4/H_2. The discharge plasma is diagnosed with well-established methods of QMS, OES and LLS. The time evolutions of gas-phase species and nanoparticle parameters of d_p and n_p are measured throughout the discharge. The polymerization and nanoparticle growth are discussed by examining the reaction rate constants and density of gas-phase species. The charging and coagulation are also discussed. Based on the observation and discussion, the followings are indicated. (i) The polysilane molecules of Si_2H_6, Si_3H_8, and Si_4H_{10} are generated via the SiH_2 insertion reactions. The densities of these molecules are $\approx 10^{14}$ cm^{-3} for Si_2H_6, $\approx 10^{13}$ cm^{-3} for Si_3H_8 and $\approx 10^{12}$ cm^{-3} for Si_4H_{10}, respectively. (ii) The clusters, i.e., nuclei of nanoparticles, are recognized at the beginning of discharge. The clusters are rapidly formed within a period of 15 ms at a high density of $\approx 10^{12}$ cm^{-3}. The size of clusters is deduced to be 1.9 nm. These clusters are formed via the insertion reactions of SiH_2 into polysilane molecules. (iii) The nanoparticles are grown in a SiH_4/H_2 plasma. For the present condition, d_p is increased from $\approx$2.0 nm at $t = 15$ ms to $\approx$10 nm at $t = 0.3$ s, and n_p is decreased from $\approx 10^{12}$ cm^{-3} at $t = 15$ ms to $\approx 3 \times 10^{10}$ cm^{-3} at $t = 0.3$ s. The mechanism of nanoparticle growth is recognized as the deposition of SiH_3 radicals on the surface. The growth rate, estimated in the model, agrees reasonably with the measured value. (iv) The generation of a large amount of nanoparticles modifies the property of plasmas. The surface of nanoparticles behaves as the recombination sites for low-energy electrons and positive ions, which induces the formation of a low-density plasma comprising high-energy electrons.

ACKNOWLEDGMENT

The authors are grateful to I. Yoshida, H. Katayama (Panasonic/Sanyo Corp.), T. Shimizu, V. Svrcek, and M. Kondo (AIST) for fruitful discussions.

REFERENCES

[1] Y. Watanabe, "Formation and behaviour of nano/micro-particles in low pressure plasmas," *J. Phys. D: Appl. Phys*., vol. 39, 2006, Art. no. R329.
[2] A. Bapat, C. Anderson, C. R. Perrey, C. B. Carter, S. A. Campbell, and U. Kortshagen, "Plasma synthesis of single-crystal silicon nanoparticles for novel electronic device applications," *Plasma Phys. Control. Fusion*, vol. 46, 2004, Art. no. B97.
[3] U. Kortshagen, "Nonthermal plasma synthesis of semiconductor nanocrystals," *J. Phys. D: Appl. Phys*., vol. 42, 2009, Art. no. 113001.
[4] P. R. i Cabarrocas, P. Gay, and A. Hadjadj, "Experimental evidence for nanoparticle deposition in continuous argon-silane plasmas: Effects of silicon nanoparticles on film properties," *J. Vac. Sci. Tech. A*, vol. 14, no. 2, pp. 655–659, 1996.
[5] T. Nozaki, K. Sasaki, T. Ogino, D. Asahi, and K. Okazaki, "Microplasma synthesis of tunable photoluminescent silicon nanocrystals," *Nanotechnology*, vol. 18, 2007, Art. no. 235603.
[6] C. H. Yang et al., "Spin-valley lifetimes in a silicon quantum dot with tunable valley splitting," *Nat. Commun*., vol. 4, no. 1, pp. 1–8, 2013.
[7] M. A. Eriksson et al., "Spin-based quantum dot quantum computing in silicon," *Quantum Inf. Process.*, vol. 3, no. 1, pp. 133–146, 2004.
[8] P. Zhao, Y. D. Lim, H. Y. Li, G. Luca, and C. S. Tan, "Advanced 3D integration technologies in various quantum computing devices," *IEEE Open J. Nanotechnol.*, vol. 2, pp. 101–110, 2021.
[9] E. C. Cho et al., "Silicon quantum dot/crystalline silicon solar cells," *Nanotechnology*, vol. 19, 2008, Art. no. 245201.
[10] X. J. Hao et al., "Synthesis and characterization of boron-doped Si quantum dots for all-Si quantum dot tandem solar cells," *Sol. Energy Mater. Sol. Cells*, vol. 93, no. 2, pp. 273–279, 2009.

[11] M. Dutta, L. Thirugnanam, P. V. Trinh, and N. Fukata, "High efficiency hybrid solar cells using nanocrystalline Si quantum dots and Si nanowires," *ACS Nano*, vol. 9, pp. 6891–6899, 2015.

[12] H. Wu, G. Zheng, N. Liu, T. J. Carney, Y. Yang, and Y. Cui, "Engineering empty space between Si nanoparticles for lithium-ion battery anodes," *Nano Lett*., vol. 12, no. 2, pp. 904–909, 2012.

[13] Y. M. Lin et al., "High performance silicon nanoparticle anode in fluoroethylene carbonate-based electrolyte for Li-ion batteries," *Chem. Commun*., vol. 48, pp. 7268–7270. 2012.

[14] M. H. Ryou et al., "Mussel-inspired adhesive binders for high-performance silicon nanoparticle anodes in lithium-ion batteries," *Adv. Mater*., vol. 25, pp. 1571–1576, 2013.

[15] R. Ohta, T. Tanaka, A. Takeuchi, M. Dougakiuchi, K. Fukuda, and M. Kambara, "Feasibility of silicon nanoparticles produced by fast-rate plasma spray PVD for high density lithium-ion storage," *J. Phys. D: Appl. Phys*., vol. 54, 2021, Art. no. 494002.

[16] M. Zacharias, J. Heitmann, R. Scholz, and U. Kahler, "Size-controlled highly luminescent silicon nanocrystals: A SiO/SiO_2 superlattice approach," *Appl. Phys. Lett*., vol. 80, no. 4, pp. 661–663, 2002.

[17] V. Svrcek, T. Sasaki, Y. Shimizu, and N. Koshizaki, "Blue luminescent silicon nanocrystals prepared by ns pulsed laser ablation in water," *Appl. Phys. Lett*., vol. 89, 2006, Art. no. 213113.

[18] M. T. Swihart, "Vapor-phase synthesis of nanoparticles," *Curr. Opin. Colloid Interface Sci.*, vol. 8, no. 1, pp. 127–133, 2003.

[19] S. Yang, W. Cai, H. Zhang, X. Xu, and H. Zeng, "Size and structure control of Si nanoparticles by laser ablation in different liquid media and further centrifugation classification," *J. Phys. Chem. C*., vol. 113, pp. 19091–19095, 2009.

[20] U. Zywietz, C. Reinhardt, A. B. Evlyukhin, T. Birr, and B. N. Chichkov, "Generation and patterning of Si nanoparticles by femtosecond laser pulses," *Appl. Phys. A*., vol. 114, no. 1, pp. 45–50, 2014.

[21] J. Valenta et al., "On the origin of the fast photoluminescence band in small silicon nanoparticles," *New J. Phys*., vol. 10, 2008, Art. no. 073022.

[22] Y. Watanabe et al., "Growth processes of particles in high frequency silane plasmas," *J. Vac. Sci. Tech. A*., vol. 14, no. 2, pp. 540–545, 1996.

[23] M. Shiratani, K. Koga, S. Iwashita, G. Uchida, N. Itagaki, and K. Kamataki, "Nano-factories in plasma: Present status and outlook," *J. Phys. D: Appl. Phys*., vol. 44, 2011, Art. no. 174038.

[24] K. Koga, Y. Matsuoka, K. Tanaka, M. Shiratani, and Y. Watanabe, "In situ observation of nucleation and subsequent growth of clusters in silane radio frequency discharges," *Appl. Phys. Lett*., vol. 77, no. 2 pp. 196–198, 2000.

[25] J. Perrin, O. Rosny, and M. C. Bordage, "Cross-sections, rate constants and transport coefficients in silane plasma chemistry," *Contrib. Plasma Phys*., vol. 36, no. 1, pp. 3–49, 1996.

[26] M. J. Kushner, "A model for the discharge kinetics and plasma chemistry during plasma enhanced chemical vapor deposition of amorphous silicon," *J. Appl. Phys*., vol. 63, pp. 2532–2551, 1988.

[27] S. Nunomura and M. Kondo, "Characterization of high-pressure capacitively coupled hydrogen plasmas," *J. Appl. Phys*., vol. 102, 2007, Art. no. 093306.

[28] S. Nunomura, I. Yoshida, and M. Kondo, "Transient phenomena in plasma-enhanced chemical vapor deposition processes of thin-film silicon," *Jpn. J. Appl. Phys*., vol. 49, 2010, Art. no. 106102.

[29] M. A. Lieberman and A. J. Lichtenberg, *Principles of Plasma Discharges and Materials Processing.* New York, NY, USA: Wiley, 1994.

[30] S. Nunomura and M. Kondo, "Positive ion polymerization in hydrogen diluted silane plasmas," *Appl. Phys. Lett*., vol. 93, 2008, Art. no. 231502.

[31] S. Nunomura, I. Yoshida, and M. Kondo, "Time-dependent gas phase kinetics in a hydrogen diluted silane plasma," *Appl. Phys. Lett*., vol. 94, 2009, Art. no. 071502.

[32] N. Konjevic, M. Ivkovic, and N. Sakan, "Hydrogen Balmer lines for low electron number density plasma diagnostics," *Spectrochimica Acta Part B*., vol. 76, pp. 16–26, 2012.

[33] J. Perrin and S. P. M. Schmitt, "Emission cross sections from fragments produced by electron impact on silane," *Chem. Phys*., vol. 67, no. 2, pp. 167–176, 1982.

[34] S. Nunomura, M. Kita, K. Koga, M. Shiratani, and Y. Watanabe, "In situ simple method for measuring size and density of nanoparticles in reactive plasmas," *J. Appl. Phys*., vol. 99, 2006, Art. no. 083302.

[35] K. Kamataki, H. Miyata, K. Koga, G. Uchida, N. Itagaki, and M. Shiratani, "Impacts of amplitude modulation of RF discharge voltage on the growth of nanoparticles in reactive plasmas," *Appl. Phys. Exp.*, vol. 4, 2011, Art. no. 105001.

[36] H. Akatsuka, "Optical Emission Spectroscopic (OES) analysis for diagnostics of electron density and temperature in non-equilibrium argon plasma based on collisional-radiative model," *Adv. Phys. X*, vol. 4, no. 1, 2019, Art. no. 1592707.

[37] T. Fujimoto, K. Sawada, and K. Takahata, "Ratio of Balmer line intensities resulting from dissociative excitation of molecular hydrogen in an ionizing plasma," *J. Appl. Phys*., vol. 66, pp. 2315–2319, 1989.

[38] S. Nunomura, M. Shiratani, K. Koga, M. Kondo, and Y. Watanabe, "Nanoparticle coagulation in fractionally charged and charge fluctuating dusty plasmas," *Phys. Plasmas*, vol. 15, 2008, Art. no. 080703.

[39] A. A. Howling, L. Sansonnens, J. L. Dorier, and C. Hollenstein, "Time-resolved measurements of highly polymerized negative ions in radio frequency silane plasma deposition experiments," *J. Appl. Phys*., vol. 75, pp. 1340–1353, 1994.

[40] T. Misawa, S. Nunomura, N. Ohno, and S. Takamura, "Observation of transverse dust lattice wave excited by unstable vertical oscillations of dust particles in an ion sheath with low gas pressure," *Jpn. J. Appl. Phys*., vol. 39, 2000, Art. no. L551.

[41] S. Nunomura, S. Zhdanov, G. E. Morfill, and J. Goree, "Nonlinear longitudinal waves in a two-dimensional screened Coulomb crystal," *Phys. Rev. E*., vol. 68, 2003, Art. no. 026407.

[42] M. Shiratani, K. Koga, S. Iwashita, and S. Nunomura, "Rapid transport of nano-particles having a fractional elementary charge on average in capacitively-coupled rf discharges by amplitude-modulating discharge voltage," *Faraday Discuss.*, vol. 137, pp. 127–138, 2008.

[43] H. Chatham, D. Hils, R. Robertson, and A. Gallagher, "Total and partial electron collisional ionization cross sections for CH_4, C_2H_6, SiH_4, and Si_2H_6," *J. Chem. Phys*., vol. 81, pp. 1770–1777, 1984.

[44] W. N. Allen, T. M. H. Cheng, and F. W. Lampe, "Ion-molecule reactions in SiH_4-D_2 mixtures," *J. Chem. Phys*., vol. 66, pp. 3371–3375, 1977.

[45] H. A. Weakliem, R. D. Estes, and P. A. Longeway, "Ion-molecule reactions in a direct current silane glow discharge," *J. Vac. Sci. Technol.: Vac., Surfaces, Films*, vol. 5, no. 1, pp. 29–36, 1987.

[46] W. M. M. Kessels, M. C. M. van de Sanden, and D. C. Schram, "Hydrogen poor cationic silicon clusters in an expanding argon-hydrogen-silane plasma," *Appl. Phys. Lett*., vol. 72, pp. 2397–2399, 1998.

[47] S. Nunomura, H. Katayama, and I. Yoshida, "Hydrogen atom kinetics in capacitively coupled plasmas," *Plasma Sources Sci. Technol.*, vol. 26, 2017, Art. no. 055018.

[48] S. Mori, Y. Katayama, and O. Sueoka, "Total cross sections for positrons and electrons colliding with SiH_4 and CF_4/S," *Atom. Collisions Res. Japan, Prog. Rep*., vol. 11, pp. 19–21, 1985.

[49] H. Tanaka, L. Boesten, H. Sato, M. Kimura, M. A. Dillon, and D. Spence, "Elastic and vibrational differential cross sections for collisions of low-and intermediate-energy electrons with silane," *J. Phys. B: At Mol. Opt. Phys*., vol. 23, 1990, Art. no. 577.

[50] H. Tawara, Y. Itikawa, H. Nishimura, and M. Yoshino, "Cross sections and related data for electron collisions with hydrogen molecules and molecular ions," *J. Phys. Chem. Ref. Data*, vol. 19, no. 3, pp. 617–636, 1990.

[51] A. Matsuda, "Microcrystalline silicon: Growth and device application," *J. Non-Cryst. Solids*, vol. 338, pp. 1–12, 2004.

[52] T. Nagai, A. H. M. Smets, and M. Kondo, "Study of spatial distribution of SiH_3 radicals in very high frequency plasma using cavity ringdown spectroscopy," *Jpn. J. Appl. Phys*., vol. 45, 2006, Art. no. 8095.

[53] K. Tachibana, T. Shirafuji, and Y. Matsui, "Measurement of SiH_2 densities in an RF-discharge silane plasma used in the chemical vapor deposition of hydrogenated amorphous silicon film," *Jpn. J. Appl. Phys*., vol. 31, 1992, Art. no. 2588.

[54] J. Perrin, Y. Takeda, N. Hirano, Y. Takeuchi, and A. Matsuda, "Sticking and recombination of the SiH_3 radical on hydrogenated amorphous silicon: The catalytic effect of diborane," *Surf. Sci*., vol. 210, no. 1/2, pp. 114–128, 1989.

[55] J. Perrin, M. Shiratani, P. Kae-Nune, H. Videlot, J. Jolly, and J. Guillon, "Surface reaction probabilities and kinetics of H., SiH_3, Si_2H_5, CH_3, C_2H_5 during deposition a-Si:H a-C:H from H_2, SiH_4, CH_4 discharges," *J. Vac. Sci. Technol. A.*, vol. 16, no. 1, pp. 278–289, 1998.